Model Diiron Protein

DOI: 10.1002/ange.200600042

The Structure of a Designed Diiron(III) Protein: Implications for Cofactor Stabilization and Catalysis**

*Herschel Wade, Steven E. Stayrook, and William F. DeGrado**

The de novo design of model metalloproteins provides a powerful approach to examine the functional consequences of metal cofactor–protein interactions.[1,2] Despite extensive work in this area, to date the structures of designed non-heme Fe proteins with bound cofactors have not been determined, rendering it difficult to fully develop structure–function relationships. Here we investigate structural properties of diiron(III) DF2t.[3] DF2t is a dimeric member of the due-ferri (DF) family of highly simplified models[3] of the more complex natural diiron enzymes. These systems, which include methane monooxygenase (MMOH),[4] ribonucleotide reductase (RNR R2),[5] and stearoyl ACP Δ^9-desaturase (Δ9D)[6] show highly similar ligand sets (almost invariably, 4-Glu,2-His) and encapsulate the diiron cofactors within four-helix bundles (Table 1).[7] As shown for the natural enzymes, DF2t binds two iron(II) ions using a 4-Glu,2-His ensemble to generate an O_2-reactive binuclear cluster. The spectroscopic properties of the diiron(III) DF2t product implicate an oxo-bridged cofactor, structurally akin to those presented by the diiron(III) enzymes.[8] The crystallographic structure of the diiron(III) DF2t cofactor is presented here, providing a simplified model of diiron enzymes.

DF2t idealizes the otherwise inexact symmetrical four-helix bundle motifs and arrangements of the Glu and His

Table 1: Diiron enzymes.

Enzyme	Abbreviation	Ligand set
methane monooxygenase	MMOH	4-Glu, 2-His
ribonucleotide R2	RNR R2	3-Glu, 1-Asp, 2-His
rubrerythrin	Rbr	4-Glu, 2-His
bacterioferritin	BFR	4-Glu, 2-His
stearoyl ACP Δ^9-desaturase	Δ9D	4-Glu, 2-His

[*] H. Wade, S. E. Stayrook, W. F. DeGrado
Department of Biochemistry and Biophysics
University of Pennsylvania
Philadelphia, PA 19104 (USA)
E-mail: wdegrado@mail.med.upenn.edu
W. F. DeGrado
Department of Chemistry
University of Pennsylvania
Philadelphia, PA 19104 (USA)
Fax: (+1) 215-573-7229

[**] We thank the National Institutes of Health (GM65416) and the NSF (DMR-05 20020 and 0425780).

Supporting information for this article is available on the WWW under http://www.angewandte.org or from the author.

ligands found in more complex diiron enzymes.[10] In aggregate, the structures of di-Mn^{II}-, di-Co^{II}-, di-Zn^{II}-, and di-Cd^{II}-bound DF variants[3b] show variations about a "canonical bis-divalent" cluster consisting of two μ-1,3-bridging Glu carboxylates, two chelating Glu carboxylates, and two $^{\delta}$N-bound His ligands (Figure 1). Each metal ion has a labile coordination

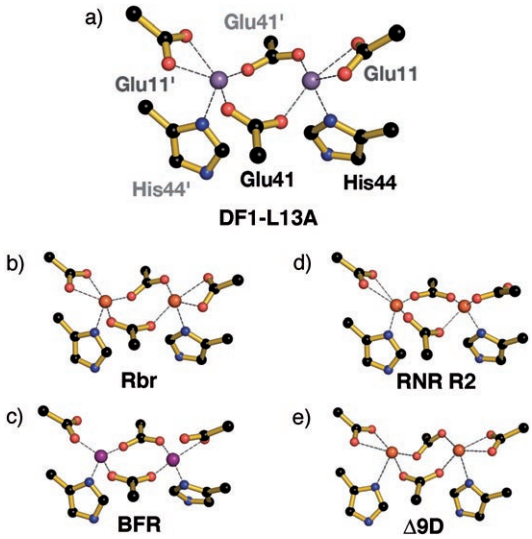

Figure 1. "Canonical bis-divalent" views of a) di-Mn^{II}·DF1L13A (1OVR), b) di-Fe^{II} Rbr (1LKO), c) di-Mn^{II} BFR (1BCF), d) di-Fe^{II} RNR R2 (1KIX), and e) di-Fe^{II} Δ9D (1AFR). The structures were generated with Pymol.[9]

position *trans* to the Fe–$^{\delta}$NHis bonds. These sites are either vacant or they can accommodate exogenous ligands in either bridging or terminal geometries. Computational studies on RNR R2 and DF2t[11] suggest that the adjacent sites are configured optimally for facile two-electron reductions of Fe-bound O_2 to peroxide. The divalent metal-bound enzyme clusters are consonant with the "canonical" view, despite showing deviations resembling "carboxylate shifts",[12] which are particularly accentuated in the diiron(III) proteins.[7,13] Smaller departures from the "canonical" view are observed in metal-bound DF proteins; the structure of diiron(III) DF2t permits the analysis of analogous deviations in a trivalent metal-bound DF complex. The structural simplicity and well-defined chemical properties of DF2t should facilitate an understanding of the minimal requirements for oxygen reactivity.

The structure of diiron(III) DF2t was solved to 2.1 Å using diffraction data collected at wavelengths shown to disfavor the photoreduction of diiron(III) enzyme centers.[15] The Fe environments (Figure 2a and Figure S1 in the Supporting Information) are consistent with those observed in diiron(III) enzymes and small-molecule models.[13,16] However, the DF2t center is more symmetric and displays fewer deviations from the "canonical" view than the diiron(III) enzyme clusters (Figure 3).[7] The close similarity between the divalent metal-bound and diiron(III) DF cofactors contrasts with the natural systems, which show more asymmetric diiron(III) centers featuring larger shifts of the Glu ligands.[17] The largest DF2t changes include minor perturbations of

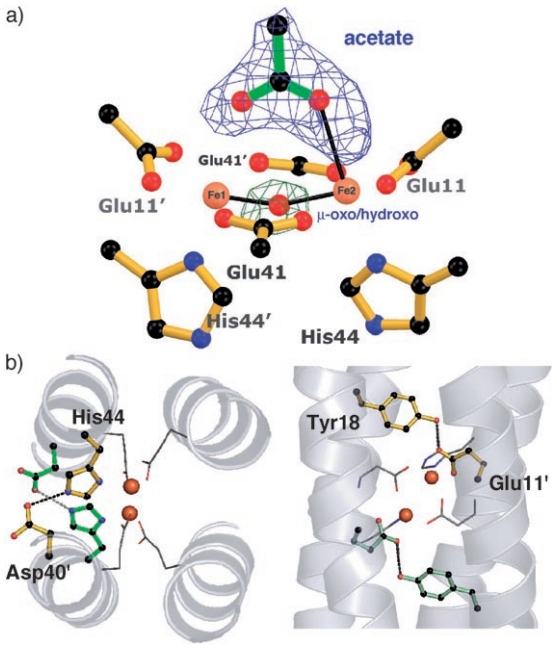

Figure 2. DF2t–cofactor interactions. a) The diiron(III) cluster ligands and σ_A-weighted F_o-F_c omit map peaks modeled by acetate and μ-oxo ligands (4.0σ). b) Second-shell hydrogen bonds (dashed lines). Symmetry-related His-Asp (right) and Tyr-Glu (left) acceptor–donor pairs are shown as ball-and-stick representations (yellow and green, respectively). Noninteracting ligands are represented by lines. The structures in part (a) were generated with Molscript and Raster3D;[14] those in part (b) with Pymol.[9]

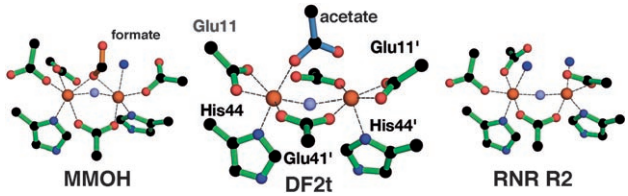

Figure 3. The Fe environments in diiron(III) DF2t, MMOH (1FZ1), and RNR R2 (1MXR). The μ-oxo/μ-hydroxo and solvent-derived ligands are depicted by light-blue and dark-blue spheres, respectively. The structures were generated with Pymol.[9]

Glu41 torsion angles, which afford Glu41 as a monodentate ligand that interacts strongly with only one iron center ($d(Fe^1\text{-}O) = 2.1$ Å; $d(Fe^2\text{-}O) = 2.4$ Å).

Two exogenous ligands were apparent from positive peaks in the electron density maps (Figure 2a). An oxo ligand was modeled at the μ-bridging position, *cis* to both Fe-$^{\delta}$NHis bonds. This assignment is consistent with the UV/Vis absorption spectrum of diiron(III) DF2t[8] and similarly bound μ-oxo/μ-hydroxo ligands observed in the diiron(III) enzymes.[16,18] As compared to natural systems, we observe an atypically wide $Fe^1\text{-}O\text{-}Fe^2$ angle of ≈146° and Fe^1–Fe^2 distance of ≈3.6 Å (vs. ≈120° and ≈3.2 Å). The Fe^1–O and Fe^2–O distances of 1.8 and 2.0 Å, respectively, are within the range typically reported for Fe^{III}-bound μ-oxo/hydroxo ligands.[7]

An acetate ion from the crystallization buffer was modeled as the other non-protein ligand (Figure 2a); acetate

is also known to bind weakly to diiron(III) DF2 in solution. The acetate coordinates to Fe^2 ($d(Fe^2–O) = 2.2$ Å) and interacts more weakly with Fe^1 ($d(Fe^1–O) = 2.4$ Å). Comparable lengthening of the Fe–Fe distance was observed in an acetate-bound diiron(III) MMOH,[19] which also showed a widened Fe-O-Fe angle and comparable $Fe–O_{oxo}$ distances. The net −1 charge on diiron(III) DF2t cluster raises the possibility of a protonated μ-oxo bridge; this is deemed less likely as the μ-oxo absorption features are only slightly diminished upon acetate binding.[20]

Significantly, acetate interacts with the Fe coordination positions occupied by peroxide in structures of DF2t and RNR R2 peroxodiiron(III) intermediates optimized by DFT.[11] Excluding the μ-oxo ligand, the acetate-bound diiron(III) DF2t cluster may recapitulate interactions implicated in catalytically relevant peroxodiiron(III) species.[21]

An extensive series of second-shell hydrogen bonds (Figure 2b) restrain the protein Glu ligands to nearly the same positions as those observed in divalent metal-bound DF proteins despite the accommodation of exogenous μ-oxo and acetate ligands. The observed rigidity does not appear to affect the reactivity of the cofactor. Stopped-flow kinetic experiments show that diiron(II) DF2t reacts rapidly with O_2, suggesting that cofactor flexibility does not influence largely the initial O_2-binding steps.[11] Although relatively rigid compared to natural systems, DF2t is able to react with O_2 and rapidly funnel the reaction towards the diiron(III) product, apparently without large nuclear motions. The larger rearrangements observed in natural systems may not be required for the initial O_2-binding steps, but instead for modulating the reactivity of enzyme–peroxo intermediates, facilitating the formation of high-valent species and promoting the oxidation of substrates.

Furthermore, the simplified DF2t cluster displays a feature that might be of structural and mechanistic relevance to natural diiron proteins. The μ-oxo ligand appears to be stabilized by second-shell CH···O hydrogen bonds[22] between the μ-oxo ligand and two $HisC^{\varepsilon}H$ groups (Figure 4). The $HisC^{\varepsilon}H$ proton is among the most acidic of the C–H groups in amino acid side chains and is potentially capable of participating in hydrogen bonds that are energetically on par with $C^{\alpha}H$···O interactions[23] proposed to play a significant role in protein stabilization.[24] Hydrogen bonds involving $HisC^{\varepsilon}H$ groups are also conserved in serine proteases, where they are believed to play an important role in catalysis.[25]

In DF2t, two $HisC^{\varepsilon}H$ groups clamp the μ ligand in pincerlike interactions. The distances and angles are restrained somewhat by the five-membered ring but lie within the ranges observed for analogous systems (Table S2 in the Supporting Information).[22] Geometrically similar interactions are present in μ-oxo/hydroxo-bridged diiron(III) and dimanganese(III) clusters of all structurally characterized O_2-activating enzymes, including dimanganene catalase[27] and toluene monooxygenase hydroxylase,[26] which displays an atypical combination of $Fe–^{\varepsilon}N$ and $Fe–^{\delta}NHis$ bonds. The $HisC^{\varepsilon}H$ pocket appears to be primed to stabilize negatively charged species; enzyme clusters that lack μ-oxo/hydroxo bridges show comparable interactions with other anionic ligands. In divalent metal-substituted enzymes, the pocket is partially filled by μ-1,1 oxygen bridges donated by coordinatively flexible Glu residues.[19,28] Moreover, an azide ion participates in two short $HisC^{\varepsilon}H$···N bonds in the diiron(II) E238A RNR R2 cluster, where the side chain of the Glu238 ligand is replaced by a methyl group.[29] Significantly, the $HisC^{\varepsilon}H$···O interactions display geometric variability among numerous diiron(III) and diiron(II) enzyme systems (Tables S2 and S3 in the Supporting Information), underscoring the flexibility to form one or two CH···O hydrogen bonds with the $HisC^{\varepsilon}H$ pair.

Possible mechanistic implications of the second-shell $HisC^{\varepsilon}H$···O interactions are shown in Scheme 1. As the metal-bound oxygen atoms are reduced to O^{2-}, the $HisC^{\varepsilon}$-H groups are positioned to stabilize the developing anionic character of oxygen atoms. Thus, $HisC^{\varepsilon}H$···O bonds resembling those found in diiron(III) enzymes structures may serve to stabilize catalytic transition states and reactive cofactor-bound intermediates, including the Q and X species.[5,30] Although CH···O hydrogen bonds are considered weak (on the order of 1 kcal mol^{-1}), they may serve to tune more energetically dominant primary interactions to specify a given reaction mechanism or product, particularly in systems such as diiron enzymes where different pathways can have comparable energetics.[4] The structural and mechanistic roles of these interactions may now be examined through theoretical and biochemical studies.

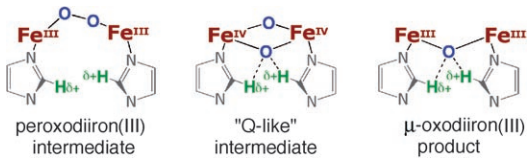

Scheme 1. The stabilization of metal-bound catalytic intermediates through $HisC^{\varepsilon}H$···O hydrogen bonds.

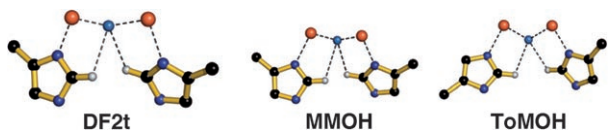

Figure 4. Second-shell interactions (dashed lines) involving $HisC^{\varepsilon}H$ atoms and μ-oxo/μ-hydroxo ligands in diiron(III) DF2t, MMOH (1FZ1), and toluene monooxygenase hydroxylase (ToMOH, 1T0S). See Table S2 in the Supporting Information for geometric details. The μ-oxo/μ-hydroxo ligands and Fe atoms are depicted by blue and orange spheres, respectively. The structures were generated with Pymol.[9]

In conclusion, the structure of diiron(III) DF2t provides the framework for further elaboration of designed diiron model proteins. The oxidized diiron DF2t cluster shows the hallmarks of natural diiron(III) enzymes and inorganic models. The center also displays unusual rigidity and is able to accommodate two additional non-protein ligands, while preserving the "canonical" appearance. Furthermore, the μ-oxo bridge has access to functionally important DF2t Fe coordination sites *cis* to both $Fe–^{\delta}NHis$ bonds, while the metal-bound acetate supports the binding capabilities of binuclear cofactors.

Experimental Section

Protein purification and crystallization: Crystals of diiron(III) DF2t (50 μM × 75 μM × 80 μM) grown by vapor diffusion using the sitting-drop method were used in the diffraction experiments. DF2t was expressed in *E. coli* and purified as previously described.[3a] Diiron-(III) DF2t was reconstituted from apo-DF2t and $Fe(NH_4)_2(SO_4)_2$ in 0.1% H_2SO_4 in 50 mM 3-(*N*-morpholine)propanesulfonic acid (MOPS), 150 mM NaCl, pH 7.0. Following the oxidation of diiron(II) DF2t, the sample was centrifuged to remove iron oxide precipitates. The sample was gel-filtered to remove nonspecifically bound Fe and dialyzed in 50 mM MOPS, 50 mM NaCl, pH 7.0. The dialysis buffer was exchanged into a salt-free 10 mM HEPES, pH 7.0 buffer by gel filtration. The final sample consisted of 1.5–2.0 mM diiron(III) DF2t. Crystals were obtained from 8.25 mM $Mg(OAc)_2$, 24–28% PEG 1500, and 100 mM HEPES, pH 7.5 at 19.0 °C. The crystals were cryoprotected by soaking in 8.25 mM $Mg(OAc)_2$, 32–36% PEG 1500, and 100 mM HEPES, pH 7.5. Crystals were obtained over four to seven days.

Diffraction data collection and refinement: The diffraction data were collected at −160° at the Advanced Light Source (beamline, 8.3.1), Lawrence Livermore Laboratories, Berkeley, CA. Data collected at 0.96 and 0.98 Å produced nearly identical models, whereas data collection at 1.08 Å produced features consistent with photoreduction (this will be reported separately). The data were integrated using DENZO and scaled with SCALEPACK. The initial phases were obtained by molecular replacement (di-Zn^{II}·DF2turn-1Y47, search model).[8] All water molecules, metal ions, and exogenous ligands were removed as the Glu ligands from the coordinate file of the search model. The initial round of refinement using the CNS suite included a rigid-body refinement, simulated annealing, conjugate gradient minimizations, and an overall B-factor refinement against maximum likelihood targets.[31] Anomalous and σ_A-weighted F_o-F_c omit difference maps were used to determine positions of the metal ions. Positional and B-factor refinements of the ions were performed using the Lennard–Jones potential for Fe^{III}. Geometrical, thermal parameter, and strict noncrystallographic symmetry (NCS) restraints were imposed during early stages of refinement and relaxed as judged by R_{free} at later stages. Well-defined electron density for all ligands was observed in maps generated with Fourier coefficients $2F_o-F_c$ and F_o-F_c and phases calculated from in-progress models built using coot and O. During later stages of refinement, σ_A-weighted $3F_o-2F_c$, $2F_o-F_c$, F_o-F_c, and composite omit maps were used to guide model building. Water picking was guided by σ_A-weighted F_o-F_c difference maps; geometric considerations and B-values served as additional validation criteria. Final rounds of refinements were performed with REFMAC5, maximum likelihood residual, anisotropic scaling, bulk-solvent correction, and the "translation, libration ,and screw rotation" (TLS) method.[31] Each DF2t monomer was treated as a rigid group, while all water molecules, metal ions, and exogenous ligands were excluded.

The final R_{work} and R_{free} values are provided in Table S1 in the Supporting Information along with rmsd values from ideal bond lengths and angles. Table S1 also lists estimated coordinate errors derived from Luzzati plots (R_{free} values) and final maximum-likelihood functions. Ramachandran plots (CCP4), WHATIF, and PROCHECK were used for validation and conformational analyses of the final models. The models exhibit good geometry with 100% of the residues in the most favored or additionally favored regions. The $Fe-N_{His}$ and $Fe-O_{Glu}$ bonds in the metal cluster are within the range expected based on data from high-resolution structures of small-molecule and protein–metal ion complexes extracted from the Cambridge Structural Database.[32]

Received: January 4, 2006
Revised: February 24, 2006
Published online: July 3, 2006

Keywords: diiron enzymes · metalloproteins · protein models · protein structures

[1] P. D. Barker, *Curr. Opin. Struct. Biol.* **2003**, *13*, 490.
[2] M. L. Kennedy, B. R. Gibney, *Curr. Opin. Struct. Biol.* **2001**, *11*, 485.
[3] a) S. J. Lahr, D. E. Engel, S. E. Stayrook, O. Maglio, B. North, S. Geremia, A. Lombardi, W. F. DeGrado, *J. Mol. Biol.* **2005**, *346*, 1441; b) J. R. Calhoun, F. Nastri, O. Maglio, V. Pavone, A. Lombardi, W. F. DeGrado, *Biopolymers* **2005**, *80*, 264.
[4] Y. Lindqvist, W. Huang, G. Schneider, J. Shanklin, *EMBO J.* **1996**, *15*, 4081.
[5] B. F. Gherman, S. J. Lippard, R. A. Friesner, *J. Am. Chem. Soc.* **2005**, *127*, 1025.
[6] J. Stubbe, P. Riggs-Gelasco, *Trends Biochem. Sci.* **1998**, *23*, 438.
[7] P. Nordlund, H. Eklund, *Curr. Opin. Struct. Biol.* **1995**, *5*, 758.
[8] O. Maglio, F. Nastri, J. R. Calhoun, S. Lahr, H. Wade, V. Pavone, W. F. DeGrado, A. Lombardi, *J. Biol. Inorg. Chem.* **2005**, *10*, 539.
[9] W. L. DeLano, Pymol, DeLano Scientific, San Carlos, CA, **2002**.
[10] A. Lombardi, C. Summa, W. F. DeGrado, *Proc. Natl. Acad. Sci. USA* **2000**, *97*, 6298.
[11] P.-P. Wei, A. J. Skulan, H. Wade, W. F. DeGrado, E. I. Solomon, *J. Am. Chem. Soc.* **2005**, *127*, 16098.
[12] R. L. Rardin, W. B. Tolman, S. J. Lippard, *New J. Chem.* **1991**, *15*, 417.
[13] D. Kurtz, *J. Biol. Inorg. Chem.* **1997**, *2*, 159.
[14] P. Kraulis, *J. Appl. Crystallogr.* **1991**, *24*, 946.
[15] A. Ericson, B. Hedman, K. O. Hodgson, J. Green, H. Dalton, J. G. Bentsen, R. H. Beer, S. J. Lippard, *J. Am. Chem. Soc.* **1988**, *110*, 2330.
[16] E. Y. Tshuva, S. J. Lippard, *Chem. Rev.* **2004**, *104*, 987.
[17] D. Whittington, S. J. Lippard, *J. Am. Chem. Soc.* **2001**, *123*, 872.
[18] B. J. Waller, J. D. Lipscomb, *Chem. Rev.* **1996**, *96*, 2625.
[19] A. C. Rosenzweig, P. Nordlund, P. M. Takahara, C. A. Frederick, S. J. Lippard, *Chem. Biol.* **1995**, *2*, 409.
[20] L. DiConstanza, H. Wade, S. Geremia, L. Randaccio, V. Pavone, W. F. DeGrado, A. Lombardi, *J. Am. Chem. Soc.* **2001**, *123*, 12749.
[21] M. Moche, J. Shanklin, A. Ghoshal, Y. Lindqvist, *J. Biol. Chem.* **2003**, *278*, 25072.
[22] T. Steiner, *Cryst. Rev.* **2003**, *9*, 177.
[23] S. Scheiner, *J. Phys. Chem. B* **2005**, *109*, 16132.
[24] A. Senes, M. Gerstein, D. M. Engelman, *J. Mol. Biol.* **2000**, *296*, 921.
[25] Z. S. Derewenda, U. Derewenda, P. M. Kobos, *J. Mol. Biol.* **1994**, *241*, 83.
[26] M. H. Sazinsky, J. Bard, A. Di Donato, S. J. Lippard, *J. Biol. Chem.* **2004**, *279*, 30600.
[27] V. V. Barynin, M. M. Whittaker, S. V. Antonyuk, V. S. Lamzin, P. M. Harrison, P. J. Artymiuk, J. W. Whittaker, *Structure* **2001**, *9*, 725.
[28] W. C. Voegtli, M. Sommerhalter, L. Saleh, J. Baldwin, J. M. Bollinger, A. C. Rosenzweig, *J. Am. Chem. Soc.* **2003**, *125*, 15822.
[29] M. Assarsson, M. E. Andersson, M. Hogbom, B. O. Persson, M. Sahlin, A. L. Barra, B. M. Sjoberg, P. Nordlund, A. Graslund, *J. Biol. Chem.* **2001**, *276*, 26852.
[30] R. A. Friesner, M. H. Baik, B. F. Gherman, V. Guallar, M. Wirstam, R. B. Murphy, S. J. Lippard, *Coord. Chem. Rev.* **2003**, *238–239*, 267.
[31] CCP4, The CCP4 Suite: Programs for Protein Crystallography, *Acta Crystallogr. Sect. D* **1994**, *50*, 760.
[32] M. M. Harding, *Acta Crystallogr. Sect. D* **1999**, *55*, 1432.

